Coarsening dynamics in uniaxial nematic liquid crystals

Issac Chuang, Bernard Yurke, and Andrew N. Pargellis
AT&T Bell Laboratories, Murray Hill, New Jersey 07974

Neil Turok
Joseph Henry Laboratories, Princeton University, Princeton, New Jersey 08544
(Received 23 November 1992)

We study the coarsening dynamics of defects in the uniaxial nematic liquid crystal 4-cyano-4′-*n*-pentylbiphenyl, subjected to a rapid pressure jump from the isotropic to the nematic phase. The defect tangle formed at the phase transition is dominated by type-$\frac{1}{2}$ strings (disclination lines), but also contains type-1 strings and monopoles. We also give a general discussion of the existence of scaling solutions to the nematodynamic equations for loop collapse and two-dimensional vortex-antivortex annihilation. We have measured the density of type-$\frac{1}{2}$ strings and loops and the monopole density as a function of time. We have also measured the rate at which the intercommutation of two strings takes place. Surprisingly, although the type-$\frac{1}{2}$ string density ρ scales as expected as a function of time, $\rho \sim t^{-1}$, loop densities and monopole densities do not seem to scale over the time interval studied. A possible explanation is given.

PACS number(s): 61.30.Jf, 64.60.Cn, 05.70.Fh

I. INTRODUCTION

There is growing interest in the coarsening dynamics of systems undergoing symmetry-breaking phase transitions involving continuous symmetries, both in condensed matter and in cosmology. The defects generated by continuous symmetry-breaking phase transitions have been invoked by cosmologists in an attempt to explain the large-scale inhomogeneity exhibited in the matter distribution of the universe [1–4]. The condensed-matter work for the most part has been theoretical with emphasis on calculating coarsening exponents [5–11]. Most of the work has concentrated on the study of models characterized by the time-dependent Landau-Ginzburg equations [9] with O(N) symmetry. For systems with a nonconserved order parameter, such models generally predict that the disclination line density in three dimensions and the vortex density in two dimensions should scale with time as t^{-1}. However, numerical simulations for three-dimensional systems have shown different scaling behaviors [9,12,13]. Numerical simulations of vortices in two dimensions find the vortex density scales as t^{-1} at late times but with a slow approach to this asymptotic scaling [6,14].

Experimental studies of the coarsening of defects have been reported for uniaxial nematic liquid crystals. The symmetry breaking in this case [15] is from global SO(3) to global O(2), resulting in a vacuum manifold (space of minimal energy configurations) which is SO(3)/O(2), the projective two-sphere. The singular defects produced during this symmetry-breaking phase transition consist predominantly of type-$\frac{1}{2}$ disclination lines. These defects belong to the π_1 homotopy class of the vacuum manifold and involve a rotation of 180° in the director field (local molecular orientation) as one goes around a closed contour encircling the disclination line. We will refer to these disclination lines as strings. In addition, there are point defects, or monopoles, which belong to the π_2 homotopy class of the vacuum manifold. One also observes nonsingular, type-1 disclination lines (strings), with the director field changing by 360°. These type-1 strings have a trivial homotopy and are therefore not true topological defects. Defects belonging to the π_3 homotopy class of the vacuum manifold are also possible. These defects are referred to as textures and candidate events have been observed [16]. It can thus be anticipated that the coarsening dynamics of uniaxial nematics is considerably more complex than the simple Landau-Ginzburg models for which the theoretical work has been done.

Orihara and co-workers [17,18] and we [19] have reported studies of the coarsening dynamics of thin films of temperature-quenched nematic liquid crystals in which twisted boundary conditions were imposed. In this two-dimensional configuration the type-$\frac{1}{2}$ strings form loops separating regions of opposite twist. This system belongs to the universality class of nonconserved Ising models with the strings serving as domain walls. The line density is expected to scale as $t^{-1/2}$. Experimentally measured coarsening exponents in the range 0.44–0.52 are close to the theoretically determined value of 0.5. We have also studied the three-dimensional coarsening of nematic liquid crystals subjected to pressure quenches [20–23]. We measured a coarsening exponent of 1.02 ± 0.09 for the type-$\frac{1}{2}$ string density, in agreement with theoretical expectations. Here we give a detailed account of our work on three-dimensional coarsening and report on observations that have not yet appeared in print. In particular, we have measured the type-$\frac{1}{2}$ string loop density and the monopole density and find that they *do not* exhibit scaling over the time interval covered by our experiments. In addition, we have measured the probabilities of line intercommutations, monopole production events, and loop

collapse events in order to obtain a detailed picture of how coarsening proceeds. At this stage, theory is not far enough developed to account for most of our observations. The coarsening dynamics of a nematic defect tangle appears to be rich, exhibiting an epoch in which loop production and monopole production is inhibited. This time period is then followed by an epoch of notable loop and monopole production.

II. THEORY: SCALING SOLUTIONS

The motion of the director field is governed by the nematodynamics equations [24]. Here, we demonstrate that those equations possess scaling solutions for collapsing director field configurations. In particular, we shall use the nematodynamic equations to show the existence of a scaling solution describing loop collapse in three dimensions and vortex pair annihilation in two dimensions (i.e., annihilation of parallel strings in three dimensions). In a previous paper we used similar arguments to find the scaling solution for monopole-antimonopole annihilation in three dimensions [25]. These scaling solutions give useful insight into more general situations involved in the behavior of the full defect tangle. For example, we show that the logarithmic corrections due to the divergence of the energy density near the core of a string actually cancel in three dimensions, but do not in two. This leads to a possible explanation of the numerical results of Mondello and Goldenfeld [6] and us [14], where it was found that the expected t^{-1} scaling for vortex density was only very slowly approached in two dimensions.

In the simplest "one-constant" approximation, and in the absence of fluid flow, the "nematodynamic" equations describing the relaxation of the liquid-crystal director in the nematic phase are given by

$$\gamma \frac{\partial n^a}{\partial t} = \kappa(\nabla^2 n^a + (\nabla n^b)(\nabla n^b) n^a) , \tag{1}$$

where $n^a(t,\mathbf{x})$ is the three-component director field, constrained to have unit length, and γ and κ are the rotational viscosity (viscoelastic) constant and elastic constant, respectively. This equation is the nonrelativistic analog of the O(N) nonlinear σ model, discussed in cosmology in connection with the spontaneous breaking of global symmetries in fundamental particle theory [26]. It also describes the relaxation of spin systems [27]. For a nematic liquid crystal n^a should be identified with $-n^a$, which will be important later.

Scaling solutions occur in partial differential equations when the solution loses dependence on the initial conditions. This often happens in the long time limit. In our case, as the loop radius R shrinks to zero, we expect the solution to lose dependence on the details of the long-wavelength modes making up the initial conditions. The same argument applies to vortex-antivortex annihilation in two dimensions. Assuming this to be true, dimensional analysis dictates that n^a can depend only on the dimensionless scaling variable $\mathbf{z}=\sqrt{\gamma/\kappa}\,\mathbf{x}/(t_0-t)^{1/2}$ where t_0 is the collapse time. In this case, the equation of motion becomes

$$\tfrac{1}{2}\mathbf{z}\cdot\nabla_z n^a = \nabla_z^2 n^a + (\nabla_z n^b)\cdot(\nabla_z n^b) n^a . \tag{2}$$

This equation follows from the stationarity of the following positive definite energy functional

$$\mathcal{E} = \int d^D z e^{-\mathbf{z}^2/4} (\nabla_z n^a)\cdot(\nabla_z n^a) \tag{3}$$

in D spatial dimensions, where one imposes the constraint $n^a n^a = 1$ either with a Lagrange multiplier, or by regarding $\mathcal{E}$ as a functional only of the two "angular" degrees of freedom in n^a.

Let us first consider a loop in three dimensions. For a loop in the $z=0$ plane centered on the z axis, we make the ansatz

$$\mathbf{n} = \cos(\Theta)\hat{\mathbf{x}} + \sin(\Theta)\hat{\mathbf{y}} , \tag{4}$$

where Θ is independent of the azimuthal angle ϕ. This describes a loop with no monopole (π_2) charge, whereas a loop produced by rigid rotation of a $+\frac{1}{2}$ string about the z axis has unit monopole charge. Now a very helpful simplification occurs. For this ansatz, we are effectively reduced to the Abelian O(2) nonlinear σ model, and it is easily seen that the evolution equation is linear in Θ. In the nematic, Θ changes by π around a string, so that $\mathbf{n}$ is not continuous, but possesses a "branch cut." However, one obtains this solution from a continuous solution describing a $+1$ singular string by dividing Θ everywhere in space by two. Since the evolution equation is linear in Θ, we still have a solution.

With this ansatz, the energy functional becomes

$$\mathcal{E} = 2\pi \int \rho\, d\rho\, dz\, e^{-(1/4)(\rho^2+z^2)} [(\partial_\rho \Theta)^2 + (\partial_z \Theta)^2] , \tag{5}$$

which has a logarithmic divergence at short distances from the string, which shall turn out to be a considerable help in determining the exact size of the scaling solution. We impose a cutoff at distance r_c from the string to make Eq. (5) finite. In a moment we shall relate r_c to the physical core radius.

Now we can make a simple argument that a stationary solution to Eq. (5) actually exists. Consider the class of configurations $\Theta(\rho,z,R)$ representing closed loops of radii R. For each value of R we imagine finding the configuration that minimizes Eq. (5), with minimal value $\mathcal{E}_{\min}(R)$. At large R, $\mathcal{E}_{\min}(R)$ falls to zero exponentially since one can choose Θ to be uniform out to a radius of order R. At small R, $\mathcal{E}_{\min}(R)$ goes to zero like $R\ln(R/r_c)$. Thus $\mathcal{E}_{\min}(R)$ goes to zero at small or large R. In fact, R parametrizes a one-parameter noncontractible loop in configuration space, as long as we identify the $R=0$ "vacuum" with that at $R=\infty$. It is then very plausible that a maximum energy point occurs on this sequence of minimal energy configurations, corresponding to a stationary point of $\mathcal{E}$. At this point we expect to find a classical solution with a single unstable mode. Note that the argument is quite general in character. We apply essentially the same argument to show the existence of a scaling solution for monopole-antimonopole annihilation [25].

Such a "mini-max" argument, which may be viewed as an application of Morse theory to infinite-dimensional configuration space, was used by Taubes to rigorously

prove the existence of a static monopole-antimonopole solution to the Yang-Mills-Higgs equations [28]. Manton then applied an analogous argument to the standard electroweak theory, which led to the construction of the "sphaleron" [29], an unstable classical solution which plays a central role in electroweak baryon number violation, a topic of much recent interest.

Before finding the detailed solution, let us interpret the unstable mode. It corresponds to a change of scale,

$$\delta n^a(\mathbf{z}) = n^a((1+\epsilon)\mathbf{z}) - n^a(\mathbf{z}) \approx \epsilon \mathbf{z}\cdot\nabla_z n^a \ . \tag{6}$$

However, $\mathbf{z}\cdot\nabla_z n^a$ is directly proportional to $(\partial n^a/\partial t)$, so the perturbation corresponds to a shift in time, and thus a shift in t_0, the annihilation time. From the time translation invariance of the equation it is clear that if a single scaling solution exists, there must be an infinite family related by time shifts. What appears as an instability in the coordinates t, $\mathbf{z}$ merely corresponds to a shift in the final collapse time t_0. This interpretation is confirmed by considering the analogous equation $(dr/dt) = 1/r$, with scaling solution $r = \sqrt{2}(t_0 - t)^{1/2}$. In terms of $z = r/(t_0 - t)^{1/2}$ and t, this exhibits the same "instability" of the scaling solution, $z = \sqrt{2}$.

Now we find the radius of the scaling solution from Eq. (5). The logarithmic divergence of Eq. (5) near the string core is of great assistance here. For a small core radius the region near the string will dominate. Thus we have

$$\mathcal{E} \simeq (2\pi)^2 R \ln(R/r_c) e^{-R^2/4} \ . \tag{7}$$

If the logarithm is large, it plays little role in determining the stationary point of Eq. (5). The stationary point actually occurs at

$$R_s \simeq \left[\frac{2\ln(R_s/r_c)}{1+\ln(R_s/r_c)} \right]^{1/2} \approx \sqrt{2} \ . \tag{8}$$

This corresponds to a scaling solution with the loop radius given by $R = \sqrt{2\kappa/\gamma}\sqrt{-t}$. This is what one expects from a naive argument based on string dynamics. The disclination lines act as strings under a tension T moving through a viscous fluid so that the friction force per unit length per unit velocity is given by Γ. Equating the viscous force with the tension force per unit length leads to the equation

$$\Gamma \frac{dR}{dt} = \frac{T}{R} \ , \tag{9}$$

where R is the loop radius as before. Integrating this equation yields

$$R = \left[\frac{2T}{\Gamma}(t_0 - t) \right]^{1/2} \ , \tag{10}$$

where t_0 is the time at which the loop vanishes. One thus expects the loop radius to shrink with time via

$$R \propto (t_0 - t)^{\alpha} \tag{11}$$

with $\alpha = 0.5$. It is not immediately apparent that this simple model should adequately describe loop collapse because the line tension of a static string is logarithmically dependent on a large distance cutoff, set by the loop radius, and because the director field relaxes diffusively. The above "mini-max" argument indicates the simple model is valid. This allows us to identify the drag force per unit length per unit velocity [30] as $(\pi/4)\gamma \ln(R/r_c)$ (four times this for a $+1$ singular string), since the string tension is given by $(\pi/4)\kappa \ln(R/r_c)$ (also multiplied by four for a $+1$ string). The logarithmic divergence in the tension has cancelled with a similar divergence in the damping force.

We now use the results for loop collapse dynamics to construct an argument for how the scaling of a random tangle of strings should proceed. When a nematic liquid crystal is subjected to a sudden pressure jump from the isotropic phase to the nematic phase, defects form as patches of fluid with uncorrelated order parameter knit together in an attempt to produce a smooth director field. This process, called the Kibble mechanism [31–33], results in a dense tangle of defects. This tangle coarsens as the fluid evolves toward equilibrium. If one assumes that the coarsening dynamics is dominated by type-$\frac{1}{2}$ strings and that the string dynamics is adequately described by the line tension T and the damping constant Γ, then a simple argument, of the Lifshitz-Slyosov type [34], which equates the time rate of change of elastic energy with the rate of energy dissipation, can be made for how the coarsening should scale with time. If one considers the defect tangle to be characterized by a single length scale ξ then the line density (length per unit volume) ρ should scale as $\rho \propto \xi^{-2}$. Equating the characteristic tension force per unit length, T/ξ, with the characteristic friction force per unit length, Γv, one finds that $v = T/\Gamma\xi$ where v is a characteristic velocity. The rate of loss of energy per unit volume is thus $\dot{W} = Tv\rho/\xi = T^2\rho^2/\Gamma$. Equating this to the time derivative of the line tension energy per unit volume, $W \propto T\rho$, gives

$$\frac{d\rho}{dt} = -c\frac{T}{\Gamma}\rho^2 \ , \tag{12}$$

where c is a constant of proportionality. Integrating Eq. (12), one finds that the scaling solution is given by

$$\rho = (\Gamma/cT)t^{-\nu} \ , \tag{13}$$

with scaling exponent $\nu = 1$.

It is not clear that the nematic liquid crystal should coarsen according to Eq. (13) since the defect tangle will, in general, consist of a mixture of defects belonging to the π_1, π_2, and π_3 homotopy classes of the vacuum manifold. As we shall now show, the energies of these different types of defects do not scale the same way with the characteristic length ξ. The energy of a defect can be calculated from the Frank free-energy density, given by [24]

$$\mathcal{F} = \tfrac{1}{2}\kappa[(\nabla\cdot\mathbf{n})^2 + (\nabla\times\mathbf{n})^2] \ , \tag{14}$$

where the surface term has been neglected. Taking $\mathbf{n} = \hat{\mathbf{r}}$ as the director field of a monopole and integrating Eq. (14) over a sphere from r_c to ξ gives $E_m = 4\pi\kappa\xi$ for the monopole energy. Similarly, the director field for a $\pm\frac{1}{2}$ string defect is $\mathbf{n} = \hat{\mathbf{x}}\cos(\phi/2) \pm \hat{\mathbf{y}}\sin(\phi/2)$. Integrating Eq. (14) over a cylinder of length and radius ξ gives

$E_{\pm 1/2}=\frac{\pi}{4}\kappa\xi\ln(\xi/r_c)$ for the type-$\frac{1}{2}$ string energy. In a similar fashion, the director field for an escaped ± 1 string is given by [35]

$$\mathbf{n}=\hat{\mathbf{x}}\cos\chi\cos\phi\pm\hat{\mathbf{y}}\cos\chi\sin\phi+\hat{\mathbf{z}}\sin\chi\ ,$$

where $\chi=2\arctan(r/\xi)$ and $r=(x^2+y^2)^{1/2}$. Integrating over a cylindrical volume gives $E_{\pm 1}=2\pi\kappa\xi$ for the energy of an escaped type-1 string. Figure 1 compares the energies of these three types of defects as a function of ξ, with the energies given in units of $\pi\kappa r_c$. As shown by the solid line in Fig. 1, the energy of a $\pm\frac{1}{2}$ string scales as $\xi\ln(\xi/r_c)$. The energy of a monopole or an escaped ± 1 string, shown respectively by the dotted and dashed lines, scales as ξ. Since the energies of different types of defects scale differently with the characteristic length ξ one expects that the system will not scale according to a single characteristic length-scale model. However, experimentally the defect tangle is seen to be dominated by type-$\frac{1}{2}$ defects. In such a case one expects approximate single length scaling for the defect tangle.

We now consider the general scaling solution to the nematodynamic equations in two dimensions, for vortex-antivortex annihilation. Consider the two-dimensional (2D) system to reside in the xz plane. The expression for the energy, Eq. (5), then loses the factor $2\pi\rho$. The same argument of the logarithmic divergence dominating now leads to

$$\mathcal{E}_{2D}\simeq 2\pi\ln\left[\frac{R}{r_c}\right]e^{-R^2/4}\ , \tag{15}$$

and the stationary point now occurs because of the logarithm. One now finds

$$R_s\simeq\left[\frac{2}{\ln(R_s/r_c)}\right]^{1/2}\ . \tag{16}$$

The physical core radius R_c is constant, so we should actually replace r_c, the cutoff in z coordinates, by a time varying cutoff $R_c\sqrt{\gamma/\kappa}/(t_0-t)^{1/2}$. This is reasonable since the time dependence of the logarithm is weak.

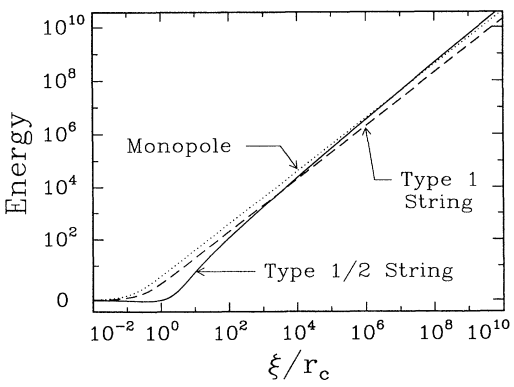

FIG. 1. A comparison of defect energies over a volume of characteristic size ξ. The energies are given in units of $\pi\kappa r_c$. The dotted, solid, and dashed lines are for the monopoles, type-$\frac{1}{2}$ strings, and type-1 strings, respectively.

With this "adiabatic" cutoff we finally obtain the scaling solution

$$R\simeq\left[\frac{2}{\ln\left[\frac{\sqrt{\kappa/\gamma}(t_0-t)^{1/2}}{R_c}\right]}\right]^{1/2}\left[\frac{\kappa}{\gamma}\right]^{1/2}(t_0-t)^{1/2}\ . \tag{17}$$

In contrast to the three-dimensional case, the logarithmic dependence remains in the two-dimensional case. While there is no logarithm in the force between a vortex-antivortex pair (which scales simply as R^{-1}), the drag force does have a logarithm. In the coarsening dynamics of the two-dimensional system, one therefore expects slower evolution at early times, with $\xi\propto\sqrt{t}\,[\ln(t/t_0)]^{1/2}$ following from the above considerations. At early times the deviation from $\sqrt{t}$ is considerable since the logarithm is changing, but at later times the logarithmic dependence becomes negligible. This observation may explain the observed time dependence of the scaling exponents seen in the two-dimensional simulations [6,14]. In three dimensions we expect that the coarsening is mainly driven by the string tension straightening curved segments of string, rather than by string-string annihilation, and therefore is most analogous to the loop collapse case above, with no logarithm entering.

III. EXPERIMENTAL RESULTS

A. Experimental apparatus

For the studies of three-dimensional coarsening reported here, the nematic liquid crystal 4-cyano-4′-*n*-pentylbiphenyl, also referred to as K15 or 5CB, was used. This molecule is rod shaped and about 30 Å long. Measurements of the splay, bend, and twist elastic constants κ_i [36] and the viscoelastic coefficient γ [37] have been reported in the literature. The material we used was obtained from BDH Limited (Poole, England) and used without further purification. At atmospheric pressure the isotropic to nematic phase transition occurs at 35.3 °C. We measured the slope $\Delta P/\Delta T$ of the coexistence curve to be 2.47 Mpa/K, between 0.7 and 17 MPa.

Figure 2 is a schematic view of the apparatus, consisting of a pressure cell with two sapphire windows. Pressure was transmitted to the cell through a Kapton diaphragm via a 15 cm length of high pressure tubing with an inner diameter of 0.75 mm. One side of the diaphragm was connected, through a valve, to a hand-turned piston containing water, the connection again being made through lengths of 0.75-mm inner-diameter high-pressure tubing. Pressure jumps were initiated by opening the valve. With this arrangement pressure jumps having a duration of less than 8 msec were obtained.

The windows of the pressure cell were treated with the homoetropic alignment material, *n*,*n*-dimethyl-*n*-octadecyl-3-aminopropyltrimethoxysilyl chloride (otherwise known as DMOAP), using standard procedures [38]. The spacing between the windows was 158 ± 8 μm for the

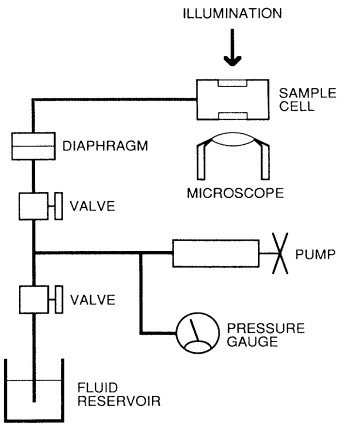

FIG. 2. A schematic of the pressure jump apparatus.

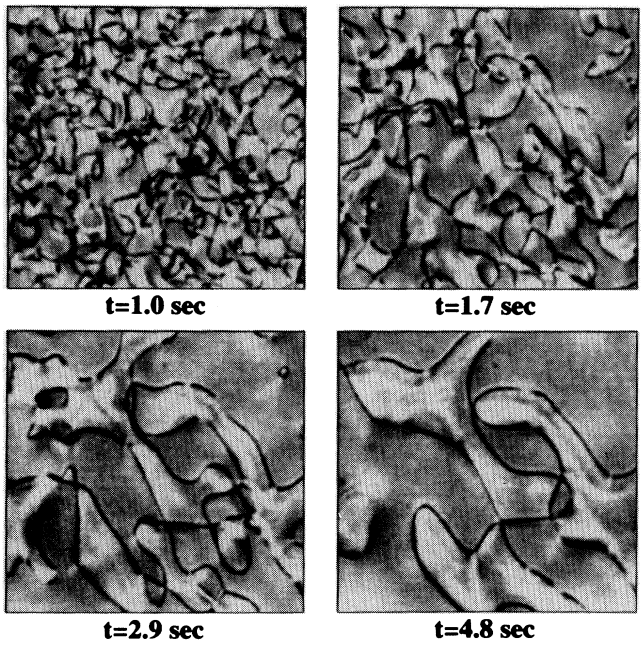

FIG. 3. A coarsening showing the strings (predominantly type-$\frac{1}{2}$) visible in our 230-μm-thick pressure cell containing K15 nematic liquid crystal, at $t=1.0$, 1.7, 2.9, and 4.8 sec after a pressure jump of $\Delta P=4.69$ Mpa from an initially isotropic state in equilibrium at approximately 37 °C and 3.6 MPa. The evolution of the string tangle shows self-similar or "scaling" behavior. Each picture is 360 μm wide.

run having a pressure jump ΔP of 2.00 MPa. For the other three runs reported here the spacing between the windows was 234±23 μm. The diameter of the sapphire plates and the sample chamber was 7 mm. The view port into the cell was 3 mm in diameter. The cell was viewed via a microscope employing backlighting. A ×10 objective having a depth of field large compared to the separation between the windows was used so that strings anywhere in the region between the two windows would be in focus. High-speed video recordings with 5 msec between frames were made of the coarsening of the pressure jump initiated defect tangles. Each video frame consisted of a 400-μm×312-μm view of the sample chamber. All the runs began at approximately the same state, at 37 °C and 3.6 MPa, but differed in the depth of the pressure jump. A sequence of 10 coarsening runs for each of the pressure jumps ΔP of 2.00, 2.28, 2.62, and 4.69 MPa were recorded. The data described here were obtained from these video recordings.

B. Coarsening of strings

We have measured the coarsening exponent ν for the type-$\frac{1}{2}$ strings and find that it is close to 1. The data were obtained by performing image processing on selected frames of the coarsening sequence. Figure 3 shows some representative frames from a coarsening sequence taken during the $\Delta P=4.7$-MPa run.

The guiding principle behind our application of image processing to clarify the string tangle pictures was to do as little processing as possible before estimating the string density. We used a four-step analysis: 3×3 median filtering, adaptive background subtraction, Sobel gradient calculation, and a cleaning algorithm similar to morphological dilation and erosion [39]. Adaptive background subtraction was accomplished by dividing the 512×400 images into 128×100 sized subimages, calculating for each region the average of each of the 32×35 subregions weighted by its standard deviation, fitting a 2D B-spline to the subimage points to get 512×400 "background" images, and subtracting these from the original images. The grey levels were then rescaled such that the mean was a light gray and the standard deviation spanned the resolution of the display. This successfully normalized the light intensity across our images. Next, we calculated the Sobel gradient image. Finally, the string density was estimated from the processed images by counting the number of points above a set threshold. Figure 4 shows the images generated from the frames of Fig. 3 with this image processing procedure.

The line density was calibrated two ways. In the first method we chose to calibrate the string density so that it represented the number of strings per unit area crossing a plane. The calibration for each data set was obtained by counting the number of strings crossing a line drawn across the image, averaged over several lines and images, and dividing by the cross-sectional area, i.e., the depth of the cell times the width of the image. In the second method we chose to calibrate the string density to represent the line length per unit volume. We selected a single set of images from the $\Delta P=2.28-$MPa run, showing the string network at $t=5.8$ sec. Using a planometer for measuring distances on a map, we measured the projected line length. Assuming that the line segments are uniformly distributed in orientation in three dimensions we obtain a line length of 88.5 mm/mm^3. This is 1.4 times larger than the string density of 55.6 mm^{-2} obtained by the first method. Note that one does not expect these two methods of obtaining a string density to give the same result since they are physically distinct. In this

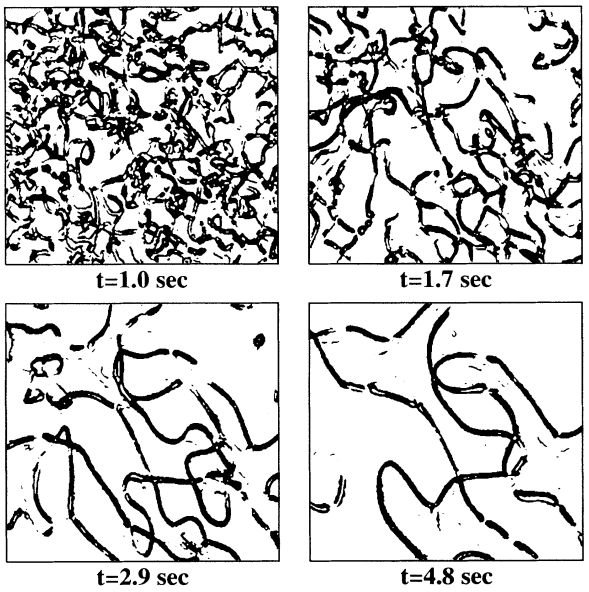

FIG. 4. Processed versions of the data in Fig. 3. The images were cleaned using 3×3 median filtering, adaptive background subtraction, Sobel gradient calculation, and morphological dilation-erosion.

manuscript the data will be presented using the second method of calibration.

Figure 5 shows the coarsening data obtained by the method described above for the four different pressure jumps ΔP. Each data point represents the average over the 10 coarsening sequences taken at each ΔP. The dotted lines scale as t^{-1}. At early and late times the data deviates from the expected t^{-1} slope. At early times the string density is sufficiently high that the method used to measure the string density underestimates the line density because of string overlap. At late times the data deviate from the expected t^{-1} behavior due to finite-size effects which will be described shortly. Omitting the first and

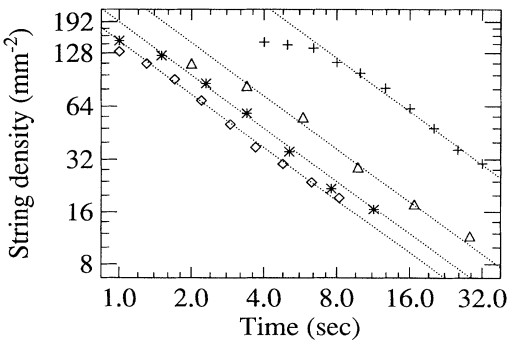

FIG. 5. String density data, accumulated at four different ΔP. Plus symbols correspond to $\Delta P=2.00$ MPa; triangles, $\Delta P=2.28$ MPa; asterisks, $\Delta P=2.62$ MPa; diamonds, $\Delta P=4.69$ MPa. The dashed lines depict a scaling of t^{-1}. By curve fitting to this data the line length per unit volume ρ was determined to scale as $\rho \propto t^{1.02\pm0.04}$.

last points from each data set, a least-squares fit gives a scaling exponent $\nu=1.02\pm0.04$, which is close to the predicted t^{-1} power law.

C. Loop collapse

In order to gain insight into the dynamics of the type-$\frac{1}{2}$ strings the collapse of nearly circular type-$\frac{1}{2}$ loops were studied. Loops with ellipticities of less than 0.6 were selected for study and the loop radius as a function of time was recorded. Such loops are generated through a sequence of intercommutation events that detach segments of type-$\frac{1}{2}$ strings from the tangle. An example of the formation of such a loop is depicted in Fig. 6. All the type-$\frac{1}{2}$ loops that we have observed during the runs reported here vanish, indicating that the loops are composed both of type-$+\frac{1}{2}$ and type-$-\frac{1}{2}$ segments. If this were not the case the loops would leave monopoles behind upon collapse.

Figure 7 shows the loop radius as a function of time for a single loop collapse. The scaling exponent in Eq. (11) for this loop was measured to be $\alpha=0.49\pm0.02$. A total of seven loops suitable for loop collapse studies were found in our data set. Averaging these results gives $\alpha=0.50\pm0.03$, in excellent agreement with our previously discussed model.

D. Loop density

As already shown in Fig. 6, during the coarsening process type-$\frac{1}{2}$ intercommutation events sometimes lead to a closed type-$\frac{1}{2}$ loop which then collapses. We measured the time of birth (the time of the intercommutation event that gave rise to the closed loop) and the time of death of type-$\frac{1}{2}$ loops of the $\Delta P=4.69$ MPa run. We included all

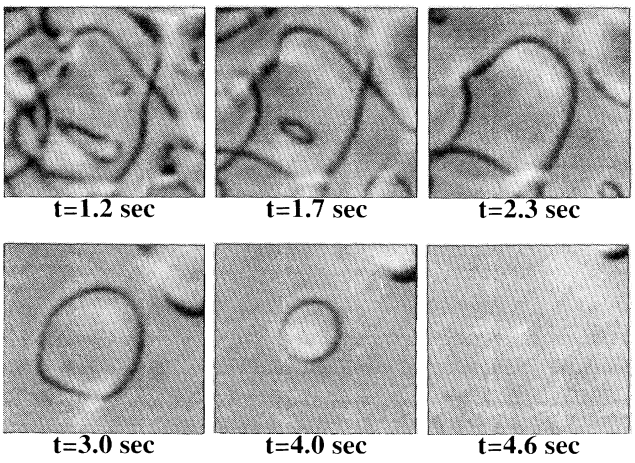

FIG. 6. Loop formation and collapse sequence. The time labels indicate the time since the pressure jump from the isotropic phase to the nematic phase. A number of intercommutations of type-$\frac{1}{2}$ strings result in the loop shown in the $t=3.0$ sec frame. The loop subsequently collapses and vanishes. The pictures were obtained from the $\Delta P=4.96$-MPa run. The width of each picture is 29 μm.

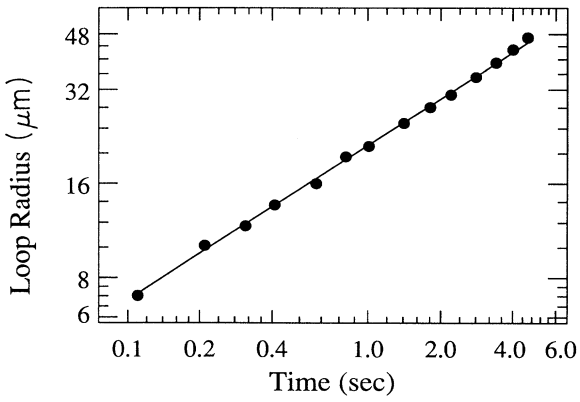

FIG. 7. Typical data showing the loop radius as a function of $t_0 - t$, where t_0 is the time at which the loop disappears. The collapse exponent for this run is $\alpha = 0.50 \pm 0.03$.

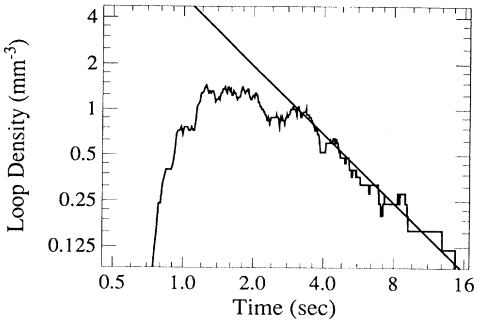

FIG. 9. Loop density ρ_l (number of loops per unit volume) as a function of time for the $\Delta P = 4.69$-MPa run. The data are complete for $t > 1$ sec. The straight line shows the expected scaling behavior $\rho \propto t^{3/2}$ expected for the bulk. Note that in the time interval between 1 and 2 sec there is a deficit in the number of loops.

type-$\frac{1}{2}$ loops that died after 1.00 sec regardless of the number of T intersections attached to them. The time lines of the loops are shown in Fig. 8. From this data one can evaluate the loop density as a function of time. Again for a system characterized by a single scaling length ξ one would expect the loop density (the number of loops per unit volume) to scale as ξ^{-3}. The loop density is thus expected to scale with time as $t^{-3/2}$. Our measured loop density is shown in Fig. 9. Note that for times greater than 3 sec the loop density exhibits the expected coarsening behavior. However, for earlier times there is a deficiency in loops. We do not attribute this deficiency to be due to experimental difficulty in identifying loops at early times. For example, at $t = 1$ sec the scale length is $\xi \approx 90$ μm. However, experimentally one is really looking at a projected image, with an average, apparent string separation (scaling length) $\xi_{\rm app} \leq \xi$. The cell thickness D needs to be considered in order to determine the relationship between the average, apparent string separation $\xi_{\rm app}$ and the average, actual string separation ξ. If one is observing strings in a volume of depth D and area ξ^2 then the measured density will be $\rho_s \sim \xi(D/\xi)/\xi^3 = D/\xi^3 \sim 1/\xi_{\rm app}^3$. Therefore, allowing for the 230 μm thickness of the cell, the observed strings should, on average, be separated by an apparent distance of $\xi_{\rm app} = [(90)^3/230]^{1/2} = 56$ μm. This distance is large compared to the 4 μm width of the image of a type-$\frac{1}{2}$ string and should be readily distinguishable in our 400-μm by 312-μm pictures. In addition, the loops are identified by running the video tapes backwards and forwards and looking for a structure that collapses to a point. Hence, we argue that the deficit in the loop density at early times is not due to obstruction by the rest of the defect tangle but is real.

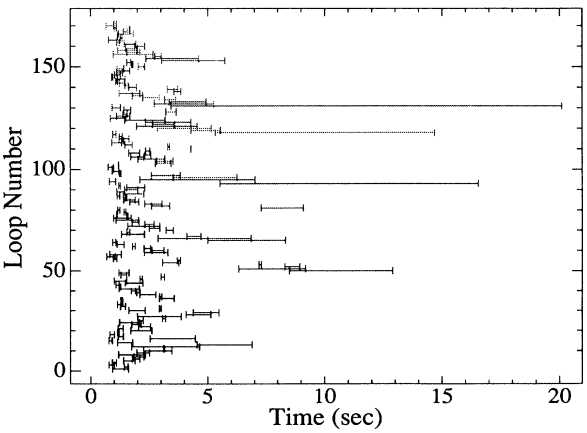

FIG. 8. Time lines of loops found in the ten pressure-jump-initiated phase transitions of the $\Delta P = 4.69$-MPa run. The data are complete for $t > 1$ sec.

E. Finite-size effects and scaling of X intersections

The analysis of the coarsening data is complicated somewhat by the finite size of the sample chamber. Because of the homoetropic alignment material used to coat the sapphire windows, the defect tangle pulls away from the windows and collapses towards the center of the sample chamber. Figure 10 shows a coarsening sequence of a defect tangle inside a capillary coated with the same homoetropic alignment material. Note that the tangle collapses toward the center of the capillary and in fact eventually becomes a single escaped type-1 string running along the center of the capillary. In the planar geometry of the sample chamber used for the coarsening experiments one expects the defect tangle to eventually decay to a two-dimensional sheet lying halfway between the two windows. The coarsening exponent for the line density of this two-dimensional sheet [15,16] will be $\nu = \frac{1}{2}$. To obtain the bulk coarsening exponent it is thus necessary to perform the line density measurements on a time scale that is short compared to the time scale on which the defect tangle collapses.

To check the degree to which the tangle has collapsed we measured the number of crossings of type-$\frac{1}{2}$ strings seen in the video frames. These crossings are not actual intersections where four string segments come together, but rather are projected images of two type-$\frac{1}{2}$ strings

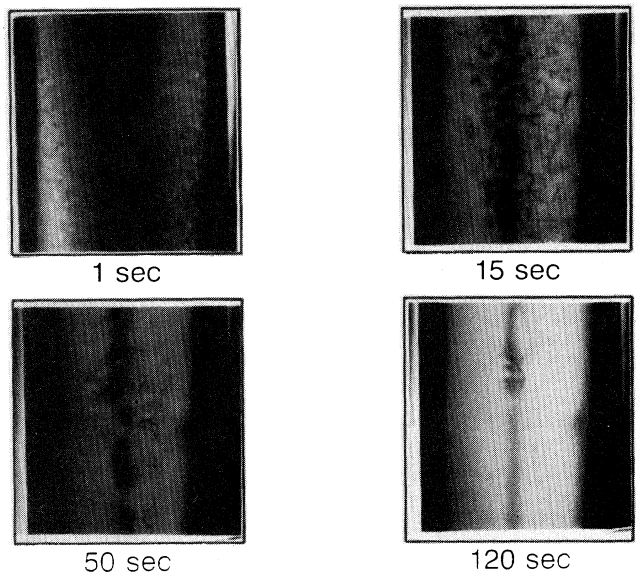

FIG. 10. Sequence showing the collapse of a defect tangle towards the center of a capillary.

crossing, one above the other. We will refer to these crossings as X intersections. These X intersections should scale as t^{-2} for the bulk if the string density scales as t^{-1}. Figure 11 shows the density of X intersections as a function of time from the $\Delta P = 4.69$-MPa run. The error bars represent the one-sigma scatter of the values for each of the eight runs analyzed. One sees that there is a definite deviation from the bulk scaling for times later than about 3 sec. If one assumes that the thickness, or path length, of the defect tangle shrinks in such a manner that the density is constant throughout the defect layer and that the tangle in this layer retains the properties of the bulk, then the time dependence of X intersections can be used to infer the thickness of the defect tangle as a function of time. This could then be used to correct the inferred string density to obtain the proper string density ρ_s. Using such a procedure, and fitting to the linear regime in the corrected $\ln\rho_s$ vs $\ln t$ data, a corrected scaling exponent of $\nu_c = 0.93 \pm 0.06$ is obtained. This number can be viewed as a lower bound on what one would expect from a more realistic model of the deviation of ν from bulk behavior for coarsening during collapse, and is thus reasonably incorporated as an additional contribution to the error bars given for our determination of the bulk scaling exponent. Our conclusion is that the scaling exponent for type-$\frac{1}{2}$ strings in bulk K15 is $\nu = 1.02 \pm 0.09$.

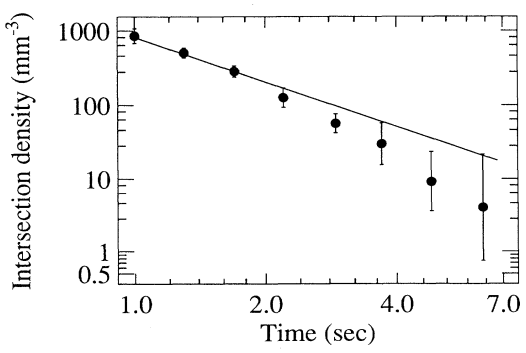

FIG. 11. X-intersection density as a function of time obtained by analyzing eight of the $\Delta P = 4.69$-MPa runs. The error bars indicate the root-mean-square deviation of the data from the mean. The solid line shows the expected t^{-2} scaling expected for the bulk.

F. Scaling of T intersections

Type-1 strings most frequently terminate on type-$\frac{1}{2}$ strings. It is possible to have closed type-1 loops but these are sufficiently rare that none were observed in the runs reported here. Figure 12 shows a sequence in which a type-1 line segment becomes absorbed in a type-$\frac{1}{2}$ string. Each end of the type-1 string terminates on the type-$\frac{1}{2}$ string. The line tension of type-$\frac{1}{2}$ strings is higher than that of the type-1 strings because the type-$\frac{1}{2}$ strings have a singular core while the type-1 strings are nonsingular. The junction of a type-1 string with a type-$\frac{1}{2}$ string thus has the shape of a "T." We will refer to these junctions as T intersections. If the scaling of the defect tangle is characterized by the single parameter ξ one expects the T-intersection density to scale as $1/\xi^3$. Hence, if the line density $\rho \sim \xi^{-2}$ scales as t^{-1}, then ξ scales as $t^{-1/2}$ and the T intersections scale as $t^{-3/2}$. Along with measuring the type-$\frac{1}{2}$ string density we measured the X-

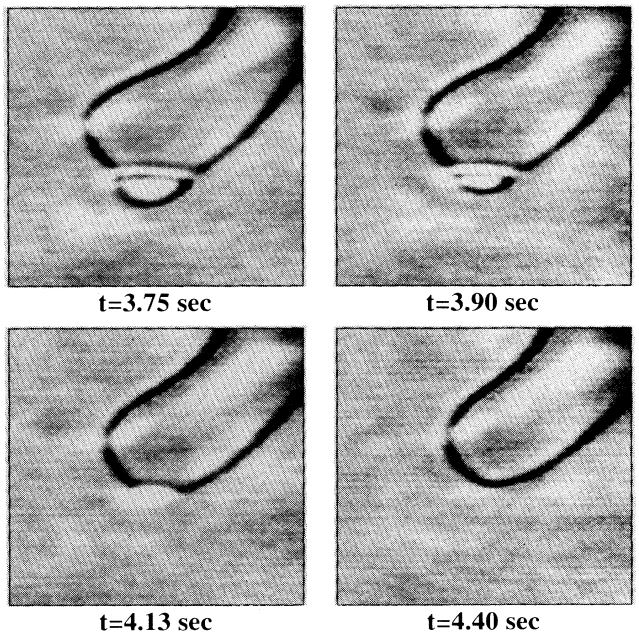

FIG. 12. Decay of a type-1 string connected two parts of the same type-$\frac{1}{2}$ string. The figure shows two T-shaped intersections that each end of the type-1 string makes where it attaches to the type-$\frac{1}{2}$ string. The pictures were obtained from the $\Delta P = 4.69$-MPa run. The width of each picture is 81 μm.

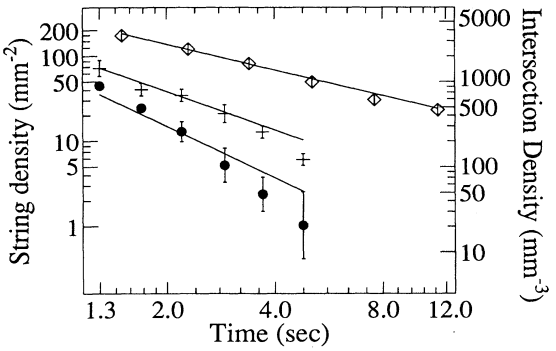

FIG. 13. Experimental data obtained from the $\Delta P = 2.62$-MPa run showing the time dependence of the type-$\frac{1}{2}$ string density ρ_S (diamonds), the T-intersection density ρ_T (plus symbols), and the X-intersection density ρ_X (filled circles). The lines depict the expected bulk scaling behavior for these quantities: $\rho_S \propto t^{-1}$, $\rho_T \propto t^{-1.5}$, and $\rho_X \propto t^{-2}$.

intersection and T-intersection density for the $\Delta P = 2.62$-MPa run. The data are depicted in Fig. 13. Also depicted are lines exhibiting t^{-1}, $t^{-3/2}$, and t^{-2} scaling. The scaling exponent for the time dependence of the T-intersection density was measured to be 1.60 ± 0.06, which is larger than the expected 1.5, perhaps again because of the finite-size effects previously mentioned.

G. Monopole density

Figure 14 shows the formation and annihilation of a monopole. In this particular sequence the monopole is created by the collapse of a type-$\frac{1}{2}$ loop with two type-1 strings coming off it. Monopoles are created by other mechanisms as well. For example, two neighboring T intersections on a type-$\frac{1}{2}$ string can merge, resulting in the detachment from the type-$\frac{1}{2}$ string of a type-1 string carrying a monopole. There are also several mechanisms by which monopoles can be destroyed. The most commonly observed, depicted in Fig. 14, is that in which the monopole travels along a type-1 string to a T intersection and is annihilated at the T intersection. Again, if the coarsening is characterized by a single length scale ξ one would expect the monopole density to scale as ξ^{-3} or as $t^{-3/2}$.

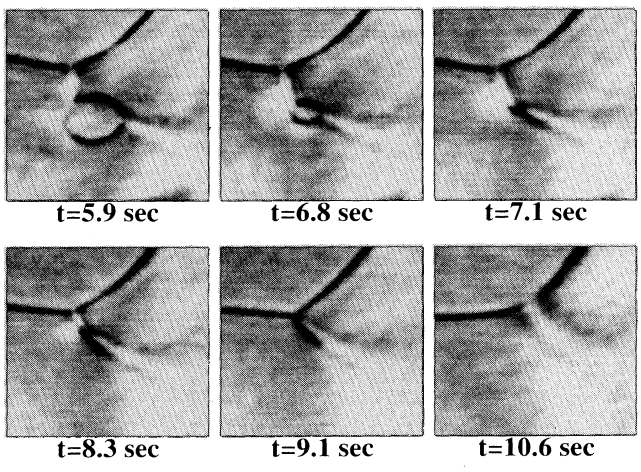

FIG. 14. Creation of a monopole from the collapse of a type-$\frac{1}{2}$ loop and its subsequent annihilation at a T intersection. The pictures were obtained from the $\Delta P = 2.28$-MPa run. The width of each picture is 96 μm.

We have recorded the time of birth and the time of death of all the monopoles in three of the four ΔP runs. From this data one can determine the monopole density as a function of time. Figure 15(a) shows the monopole density versus time for each of the three runs $\Delta P = 2.28$, 2.62, and 4.69 MPa. Figure 15(b) shows the three curves superimposed by rescaling in log-time so that the centroid of each curve is centered on that of the 4.60-MPa data. As with the loop density, the monopole density does not scale as expected. There is a relatively sudden initiation of monopole production at early times. The monopole density reaches a maximum and then decays more quickly than the $\rho_m \propto t^{3/2}$ expected from a one-scale model. In fact, a scaling of $\rho_m \propto t^3$ more accurately characterizes the late time scaling. There is thus an epoch during which monopole production turns on and an epoch during which the monopole density rapidly decays. Since type-$\frac{1}{2}$ loop collapse provides a major mecha-

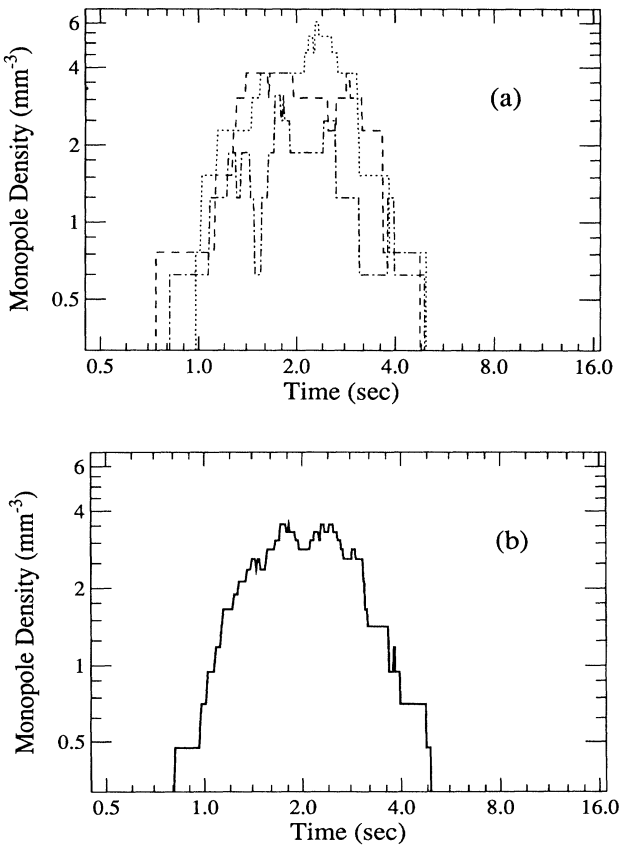

FIG. 15. (a) Monopole density ρ_m as a function of time for the runs; $\Delta P = 4.69$ MPa (dashed line), $\Delta P = 2.62$ MPa (dotted line), and $\Delta P = 2.26$ MPa (dot-dashed line). (b) Rescaled and superimposed curves of (a).

nism by which monopoles are created perhaps the deficit in monopole production is due to the deficit of type-$\frac{1}{2}$ loops at early times.

H. Scaling violations

It was previously argued in Sec. II, and summarized in Fig. 1, that the energies of different types of defects scale differently with ξ and hence the system may not exhibit scaling. In this section we propose a possible explanation for the observed deviations of the monopole and loop densities from scaling. This argument relies on the coincidence that the attractive force between two strings, with a logarithmic dependence on their separation, dominates their repulsive force soon after the point where the defect tangle becomes clearly resolved. If confirmed, it will provide a rather remarkable instance where a very large length and time scale is produced in an otherwise "scale-free" system through a logarithm.

The main point is that the formation of a new monopole requires the self-intersection of a type-$\frac{1}{2}$ string, thus forming a loop having a monopole charge. The resulting closed loop collapses to form the monopole. However, type-$\frac{1}{2}$ strings, separated a distance d, actually repel [24], with a force per unit length, $F_r \propto \kappa/d$. The attractive force per unit length, $F_a \propto T/R$, pulls a string towards a self-intersection, where R is the radius of curvature of the string. Since the tension T is the energy per unit length along the string, the attractive force is $F_a \propto (\kappa/R)\ln(d/r_c)$. At any time, the typical configuration would have $d \sim R \sim \xi$, the characteristic scale on the network. However the tension scales logarithmically with ξ, whereas the repulsive force does not. The "crossover" scale length $\xi = r_c e^A$ occurs when $F_r = F_a$, where A is a proportionality constant. For larger scale lengths, $F_a > F_r$ and closed loops and monopoles will start to form. Using the value of $\xi \simeq 90$ μm at $t = 1$ sec and setting $r_c \sim 30$ Å for the length of the liquid-crystal molecule gives $A \sim 10$.

Close observations of video recordings of the network show the process rather clearly. At times before 1 sec, the string appears to avoid itself when a self-intersection seems imminent, but after this time self-intersections occur readily. We can write down an equation for the production of monopoles, with a number density n_m, as

$$\frac{dn_m}{dt} = +\frac{C}{t\xi^3}\ln\left[\frac{t}{t_c}\right], \quad t > t_c \ . \tag{18}$$

C is an unknown constant of proportionality, and t_c is the critical time. We use the fact that the only length and time scale are provided by $\xi \propto t^{1/2}$. This equation is solved to obtain the total accumulated number of monopoles at time t,

$$n_m(>t) = C'\left\{1 - \left[\frac{t_c}{t}\right]^{3/2}\left[1 + \frac{3}{2}\ln\left[\frac{t}{t_c}\right]\right]\right\} \tag{19}$$

with C' a constant. We have calculated the accumulated number of monopoles in each run, ignoring annihilations, from the data, rescaling the time in each run by a constant factor. This factor is chosen so that after rescaling, the string densities shown in Fig. 5 are equal in all runs to the string density in the $\Delta P = 4.69$-MPa run. With this rescaling of the time, and the scaling hypothesis, we should remove all dependence on the pressure used in each run. Figure 16 shows the scaled results of the data shown in Fig. 15, taken for three different pressure jumps. The curves are the fits of Eq. (19) to the data sets. The fit is quite good, but we have used two free parameters, the constant $C' \simeq 14.5$ and the time $t_c \simeq 0.66$ sec.

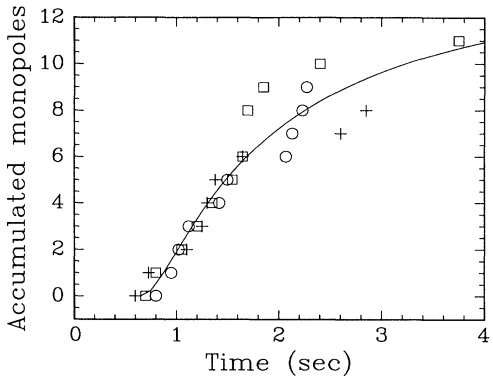

FIG. 16. The cumulative number of monopole births as a function of time for the rescaled data of Fig. 15(b). The curve is a fit to Eq. (19).

We do not regard our proposed explanation as definitive, but it does bear further investigation. If it turns out to be correct, it will provide a remarkable instance of a large length scale being dynamically generated through a logarithm. Similar phenomena could well occur in cosmological theories.

I. Event statistics

The motion of strings in a defect tangle is one that reduces the total line tension energy. Hence the strings generally move to increase the local radius of curvature and straighten themselves out. Also, as in loop collapses, the strings move in a manner that shortens line length. Both these processes continuously reduce the line length of the defect tangle. Besides this continuous motion there are events that take place at well-defined instances of time, such as the intercommutation of two strings, the creation of a monopole, the collapse of a loop, etc. We have constructed a classification of these discrete events and have measured their relative probabilities of occurrence. The data was obtained for the $\Delta P = 4.69$-MPa run. All events occurring later than 2 sec were recorded. For times earlier than 2 sec only one-fourth of the video frame area was searched for events. In this data set we have identified 16 different types of events, listed in Table I. Note that type-1 strings are depicted as a pair of parallel lines. This is not an exhaustive list of the kinds of events that can be observed in uniaxial nematic liquid crystals. Therefore, Table I is only a list of the 16 most abundant types of events. For example, not included in

TABLE I. Event classification list. The first column gives the identification number we have given each type of event.

Code	Event pictograph	Description
1	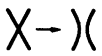	Intercommutation of two $\pm\frac{1}{2}$ strings (The two initial strings are separated in space)
2	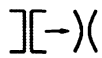	Decay of a ±1 across two $\pm\frac{1}{2}$'s into two $\pm\frac{1}{2}$'s
3	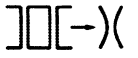	Decay of two ±1's across two $\pm\frac{1}{2}$'s into two $\pm\frac{1}{2}$'s
4	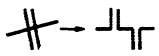	Intercommutation of a $\pm\frac{1}{2}$ and a ±1 resulting in a $\pm\frac{1}{2}$ with two T intersections
5	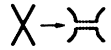	Intercommutation of two $\pm\frac{1}{2}$'s resulting in two $\pm\frac{1}{2}$'s connected by a ±1
6	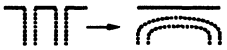	Unlinking of two ±1's from a $\pm\frac{1}{2}$
7	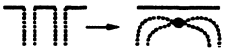	Unlinking of two ±1's from a $\pm\frac{1}{2}$ resulting in a single $\pm\frac{1}{2}$ and a monopole carrying ±1
8	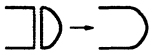	Decay of a ±1 connecting two parts of the same $\pm\frac{1}{2}$ into a single $\pm\frac{1}{2}$
9	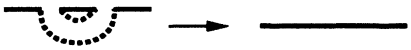	Decay of a ±1 connected at both ends to a straight segment of a $\pm\frac{1}{2}$
10	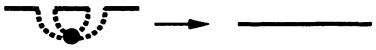	Decay of a monopole carrying ±1 connected at both ends to a straight segment of a $\pm\frac{1}{2}$
11	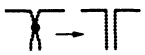	Decay of a monopole sitting on a ±1 by absorption into a $\pm\frac{1}{2}$
12	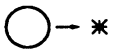	Collapse of a $\pm\frac{1}{2}$ loop (no end products)
13	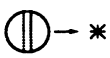	Collapse of a $\pm\frac{1}{2}$ loop with a ±1 across it
14	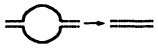	Collapse of a $\pm\frac{1}{2}$ loop with two ±1's coming out at either end, resulting in a single ±1
15	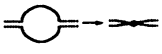	Collapse of a $\pm\frac{1}{2}$ loop, with two attached ±1's, resulting in a monopole carrying ±1
16	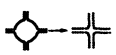	Collapse of a $\pm\frac{1}{2}$ loop with four attached ±1's resulting in a four-(±1) vertex which escapes

this list is the annihilation of a monopole and an antimonopole. We have observed such events to be quite common in cylindrical geometries [25], but here they occur at a sufficiently low frequency that no examples were found in the runs reported here. Another example is the collapse of a type-1 loop. This is very rare even when, through doing a slow pressure or temperature quench, conditions are optimized for type-1 loop creation.

We have created a classification scheme for these

TABLE II. Events, their probabilities, and associated classification numbers. The event probabilities for $t < 2.0$ sec were determined from a total of 131 events. The event probabilities for $t > 2.0$ sec were determined from a total of 354 events. The data were from the $\Delta P = 4.60$-MPa run.

Code	Event	% Prob.	Δn_T	Δn_M	Δn_L	Δn_{1s}	$\Delta n_{(1/2)s}$
1	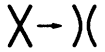	26.6					
2	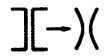	10.3	−2		−1	−1	
3		1.0	−4		−1	−2	
4	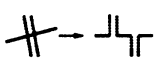	0.2	+2		+1		
5	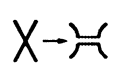	0.2	+2		+1	+1	
6	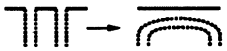	8.9	−2		−1		
7	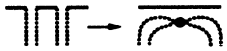	0.6	−2	+1	−1		
8	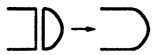	25.8	−2			−1	
9	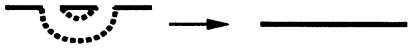	1.7	−2			−1	
10	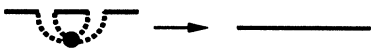	0.8	−2	−1		−1	
11	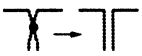	2.3		−1			
12	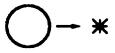	8.9					−1
13	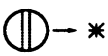	1.2	−2			−1	−1
14	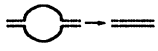	5.8	−2				−1
15	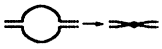	1.4	−2	+1			−1
16	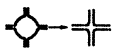	0.4	−4				−1

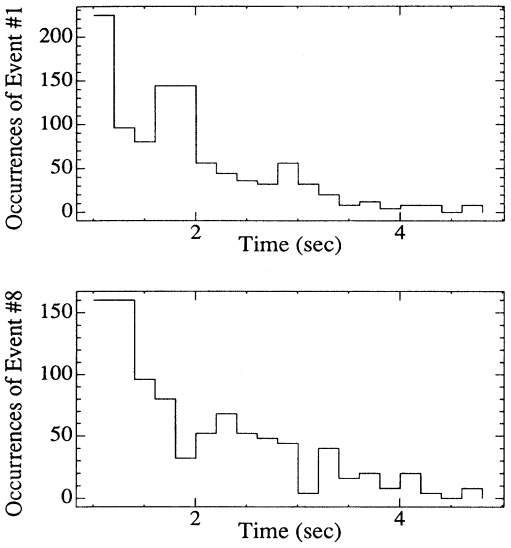

FIG. 17 The number of occurrences of events of type 1 and type 8 as a function of time for the $\Delta P = 4.69$-MPa run. The type-1 events are intercommutations of type-$\frac{1}{2}$ strings. The type-8 events are the annihilation of type-1 line segments by type-$\frac{1}{2}$ strings as depicted in Fig. 13.

events based on the changes these events make to the defect tangle. This is depicted in Table II, which also displays the relative probability that an event takes place for the time interval $1.0 < t < 2.0$ sec and for the time interval $2.0 \leq t < 5$ sec. All events (a total of 354 events) occurring in the 440-μm$\times$312-μm view area of the video frames were recorded for the time interval from 2.0 to 5.0 sec. For the time interval between 1.0 and 2.0 sec only one-quarter of each frame was examined for events; a total of 131 events were found in this interval.

The classification scheme is defined as follows. Δn_T is the difference in the number of T intersections before and after the event takes place. Δn_M is the change in the number of monopoles after the event takes place. Δn_{1s} and $\Delta n_{(1/2)s}$ are the change in the number of type-1 and type-$\frac{1}{2}$ lines in the local vicinity of the event. Note that events 8 and 9 are not topologically distinct but are generally easy to distinguish depending on whether the type-$\frac{1}{2}$ or the type-1 string exhibits greater curvature. A total of 485 events were observed. Of this number only 3.9% were unclassifiable due to obscuration. Over the time interval from 1 to 5 sec the most abundant event, event 1 in Table II, consists of the intercommutation of type-$\frac{1}{2}$ strings. The second most abundant event is event 8 in which a type-1 and a type-$\frac{1}{2}$ string combine to form a single type-$\frac{1}{2}$ string. The number of these two most abundant events as a function of time is shown in Fig. 17. In this figure, the events occurring earlier than 2 sec have been multiplied by 4 to normalize them to the data for times greater than 1 sec.

IV. CONCLUSIONS

We have studied the coarsening of the defect tangle in a uniaxial liquid crystal. The type-$\frac{1}{2}$ string density scales as expected from simple models and from theoretical work that has been done on the coarsening of strings. This is perhaps due to the fact that the type-$\frac{1}{2}$ strings are the most energetic and dominate the dynamics of the defect tangle. However, the loop density and monopole density do not appear to scale in a simple way. This is surprising since there is only one characteristic length scale in the liquid crystal, the core size of a type-$\frac{1}{2}$ disclination line which is of the order of 30 Å, much smaller than the length scales observed in our experiment. As we argued in Sec. III H, there is a possible mechanism through which the 30 Å length scale can generate a much larger length scale, provided by the logarithmic dependence of the string tension on the correlation length scale ξ. We have seen that a rate equation built on this explanation provides a reasonable fit to the data.

Modeling and explaining the detailed results including those of the last section is a task for the future. In particular, more and better data are desired in order to improve our understanding of the event statistics of liquid-crystal defects.

ACKNOWLEDGMENTS

We thank R. Durrer and P. E. Cladis for helpful discussions. N. T. acknowledges the support of NSF Grant No. PHY80-19754 and the Alfred Sloan Foundation.

[1] A. Vilenkin, Phys. Rep. **121**, 263 (1985).
[2] N. Turok, Phys. Rev. Lett. **63**, 2625 (1989).
[3] C. T. Hill, D. N. Schramm, and J. N. Fry, Comments Nucl. Part. Phys. **19**, 25 (1989).
[4] W. H. Press, B. S. Ryden, and D. N. Spergel, Astrophys. J. **347**, 590 (1989).
[5] P. C. Hohenberg and B. I. Halperin, Rev. Mod. Phys. **49**, 435 (1977).
[6] M. Mondello and N. Goldenfeld, Phys. Rev. A **42**, 5865 (1990).
[7] H. Toyoki and K. Honda, Prog. Theor. Phys. **78**, 237 (1987).
[8] H. Toyoki, Phys. Rev. A **42**, 911 (1990).
[9] H. Nishimori and T. Nukii, J. Phys. Soc. Jpn. **58**, 563 (1988).
[10] F. de Pasquale and P. Tartaglia, Phys. Rev. B **333**, 2081 (1986).
[11] G. F. Mazenko and M. Zannetti, Phys. Rev. B **32**, 4565 (1985).
[12] M. Mondello and N. Goldenfeld, Phys. Rev. A **45**, 657 (1992).
[13] R. E. Blundell and A. J. Bray, Phys. Rev. A **46**, 6154 (1992).
[14] A. N. Pargellis *et al.*, Phys. Rev. A **46**, 7765 (1992).
[15] M. Kleman, L. Michel, and G. Toulouse, J. Phys. Lett. (Paris) **38**, L195 (1977).

[16] Y. Bouligand, *Physics of Defects,* edited by R. Balian, M. Kleman, and J. Poirier (North-Holland, Amsterdam, 1981), pp. 665–711.
[17] H. Orihara and Y. Ishibashi, J. Phys. Soc. Jpn. **55**, 2151 (1986).
[18] T. Nagaya, H. Orihara, and Y. Ishibashi, J. Phys. Soc. Jpn. **56**, 3086 (1987).
[19] N. Mason, A. N. Pargellis, and B. Yurke, Phys. Rev. Lett. **70**, 190 (1993).
[20] I. Chuang, R. Durrer, N. Turok, and B. Yurke, Science **251**, 1336 (1991).
[21] I. Chuang, N. Turok, and B. Yurke, Phys. Rev. Lett. **66**, 2472 (1991).
[22] I. Chuang, Master's thesis, Massachusetts Institute of Technology, 1991 (unpublished).
[23] R. Snyder *et al.,* Phys. Rev. A **45**, R2169 (1992).
[24] P. G. de Gennes, *Liquid Crystals* (Clarendon, Oxford, 1974).
[25] A. Pargellis, N. Turok, and B. Yurke, Phys. Rev. Lett. **67**, 1570 (1992).
[26] N. Turok and D. Spergel, Phys. Rev. Lett. **66**, 3093 (1991).
[27] T. J. Newman, A. J. Bray, and M. A. Moore, Phys. Rev. B **42**, 4514 (1990).
[28] C. H. Taubes, Commun. Math. Phys. **86**, 257 (1982); **86**, 299 (1982).
[29] N. S. Manton, Phys. Rev. D **28**, 2019 (1983); F. Klinkhamer and N. Manton, *ibid.* **30**, 2212 (1984).
[30] G. Ryskin and M. Kremenetsky, Phys. Rev. Lett. **67**, 1574 (1991).
[31] T. W. B. Kibble, J. Phys. A **9**, 1387 (1976).
[32] T. W. B. Kibble, Phys. Rep. **67**, 183 (1980).
[33] W. H. Zurek, Nature (London) **317**, 505 (1985).
[34] I. M. Lifshitz, and V. V. Slyosov, J. Phys. Chem. Solids **19**, 35 (1961).
[35] P. E. Cladis and M. Kleman, J. Phys. (Paris) **33**, 591 (1972).
[36] P. P. Karat and N. V. Madhusdana, Mol. Cryst. Liq. Cryst. **40**, 239 (1977).
[37] Shin-Tson Wu and R. J. Cox, J. Appl. Phys. **64**, 821 (1988).
[38] F. J. Kahn, Appl. Phys. Lett. **22**, 386 (1973).
[39] R. C. Gonzalez and P. Wintz, *Digital Image Processing* (Addison-Wesley, Reading, MA, 1987).

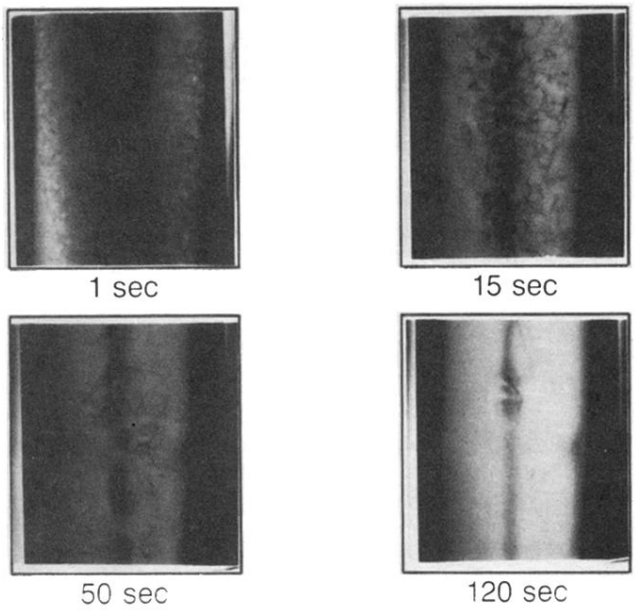

FIG. 10. Sequence showing the collapse of a defect tangle towards the center of a capillary.

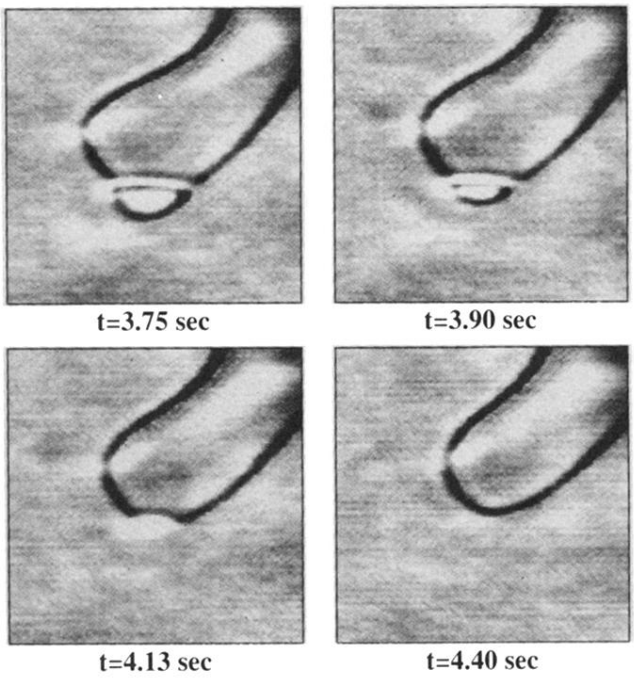

FIG. 12. Decay of a type-1 string connected two parts of the same type-$\frac{1}{2}$ string. The figure shows two T-shaped intersections that each end of the type-1 string makes where it attaches to the type-$\frac{1}{2}$ string. The pictures were obtained from the $\Delta P = 4.69$-MPa run. The width of each picture is 81 μm.

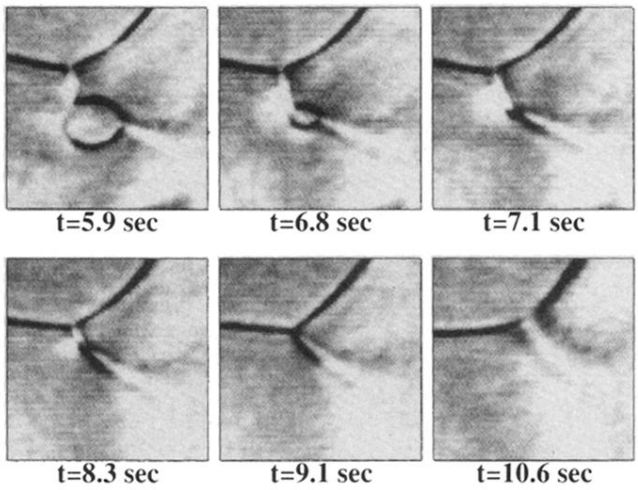

FIG. 14. Creation of a monopole from the collapse of a type-$\frac{1}{2}$ loop and its subsequent annihilation at a T intersection. The pictures were obtained from the $\Delta P = 2.28$-MPa run. The width of each picture is 96 μm.

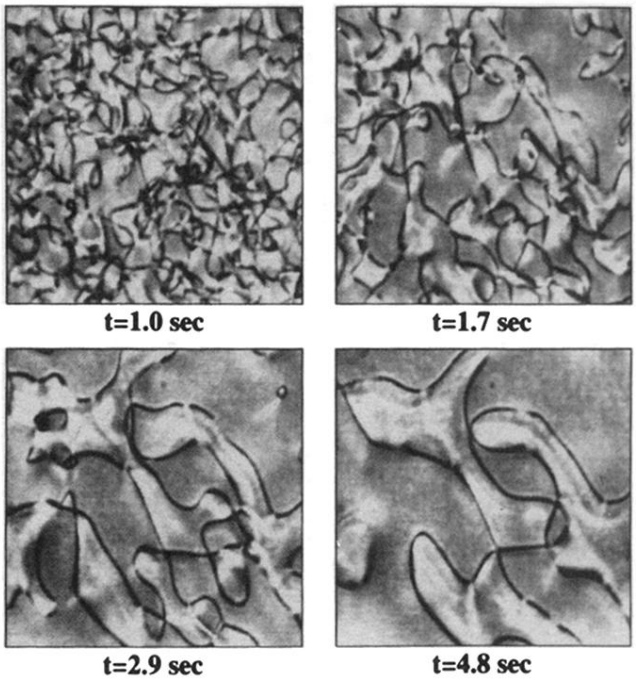

FIG. 3. A coarsening showing the strings (predominantly type-$\frac{1}{2}$) visible in our 230-μm-thick pressure cell containing K15 nematic liquid crystal, at $t=1.0$, 1.7, 2.9, and 4.8 sec after a pressure jump of $\Delta P=4.69$ Mpa from an initially isotropic state in equilibrium at approximately 37 °C and 3.6 MPa. The evolution of the string tangle shows self-similar or "scaling" behavior. Each picture is 360 μm wide.

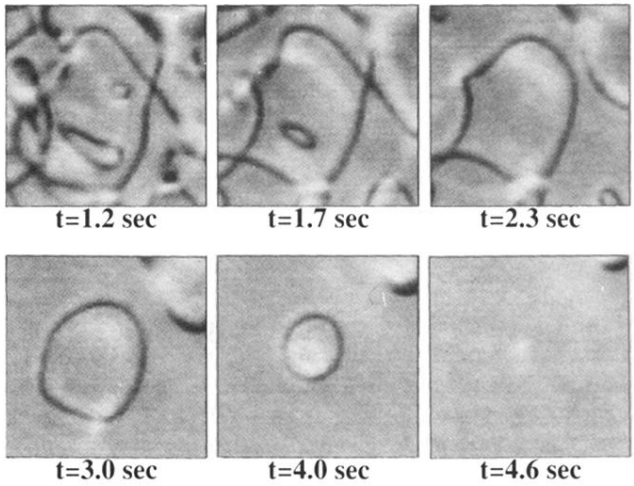

FIG. 6. Loop formation and collapse sequence. The time labels indicate the time since the pressure jump from the isotropic phase to the nematic phase. A number of intercommutations of type-$\frac{1}{2}$ strings result in the loop shown in the $t=3.0$ sec frame. The loop subsequently collapses and vanishes. The pictures were obtained from the $\Delta P=4.96$-MPa run. The width of each picture is 29 μm.